Supplement of Atmos. Chem. Phys., 25, 1931–1947, 2025
https://doi.org/10.5194/acp-25-1931-2025-supplement

Atmospheric Chemistry and Physics
Open Access
EGU

Supplement of

Cloud processing of dimethyl sulfide (DMS) oxidation products limits sulfur dioxide (SO_2) and carbonyl sulfide (OCS) production in the eastern North Atlantic marine boundary layer

Delaney B. Kilgour et al.

Correspondence to: Timothy H. Bertram (timothy.bertram@wisc.edu)

S1 HPMTF detection, calibration, and uncertainty

The Vocus AIM sampled from a 4 m inlet height, roughly 1 m above the top of the trailer, through a 4.5 m long 1/2″ O.D., 11 mm I.D. PFA tube. The full inlet tube was pumped at 10 lpm, resulting in an inlet residence time of about 2.6 s. The in-field $I•H_2O^-:I^-$ ratio was 0.97 ± 0.06 for iodide reagent ion mode on the Vocus AIM. The formic acid sensitivity at an $I•H_2O^-:I^-$ ratio of 0.97 was 4.55 ncps ppt^{-1}, normalized per million of reagent ion counts, and determined via humidity-dependent formic acid calibrations on this instrument. The instrument's sensitivity to formic acid was expected to be a reasonable approximation for its sensitivity to HPMTF, as the iodide adduct binding enthalpies for HPMTF and formic acid are similar (-25.05 kcal mol^{-1} for HPMTF and -25.52 kcal mol^{-1} for formic acid) (Iyer et al., 2016; Jernigan et al., 2022a). The mass resolution (*m/Δm)* of the Vocus AIM was ~5500, which allowed for separation of HPMTF ($[C_2H_4SO_3•I]^-$, 234.8931) from other ions at the same nominal mass, (234.8655, 234.9109 (suggested as $[CH_3COOH•IO_3]^-$), 234.9434, and 234.9811). The exception was $N_2O_5•I^-$ (234.8857), though the potential contribution of this ion on the presented analysis was estimated as minimal (see main text).

We tested the validity of the HPMTF calibration factor by comparing clear sky measurements of HPMTF to a chemical box model developed in F0AM. This comparison was completed for July 11, 2022, where the mean and standard deviation in CF_{3A} (Hr. 6-17) were 0.065 ± 0.055 and the mean and standard deviation in DMS over the entire day were 45 ± 31 ppt. The box model was constrained by observed meteorological conditions and trace gas measurements on this day. A DMS flux was specified to match the day's average measured DMS concentration. This comparison indicates that the reported HPMTF concentrations, calibrated with formic acid, are a lower limit, and could underrepresent ambient HPMTF concentrations by up to 60% (Fig. S1). The model-measurement disagreement in absolute HPMTF concentrations arises from uncertainty in the calibration factor and inlet loss of HPMTF. Given the ambient relative humidity was always greater than 50%, and typically much higher (campaign mean and standard deviation of 80±8%), and the ICIMS $I•H_2O^-:I^-$ ratio was relatively constant, we expect uncertainty in HPMTF provides a systematic error. This means that trends reported here with 3-dimensional cloud fraction are expected to be robust.

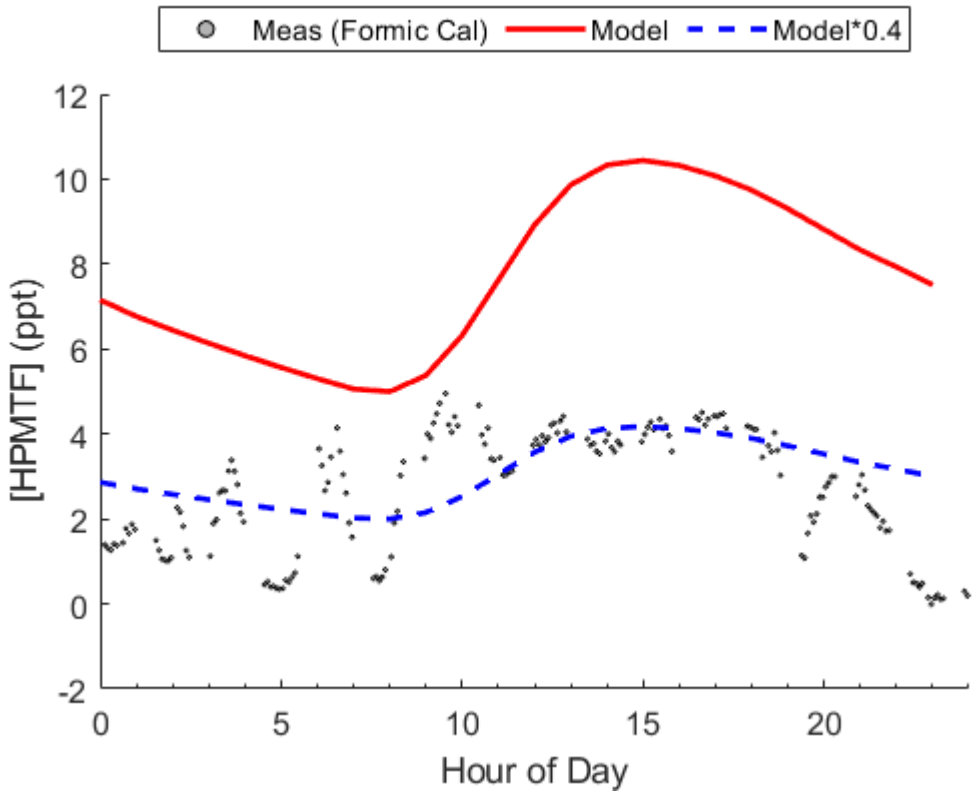

Figure S1: Measurements of HPMTF, calibrated with the formic acid calibration factor, on July 11th are shown with dots. The modelled HPMTF concentration, in red, for a clear sky model constrained by measurements on July 11th. Measured HPMTF could be underestimated by 60%, due to a combination of calibration factor uncertainty and inlet loss.

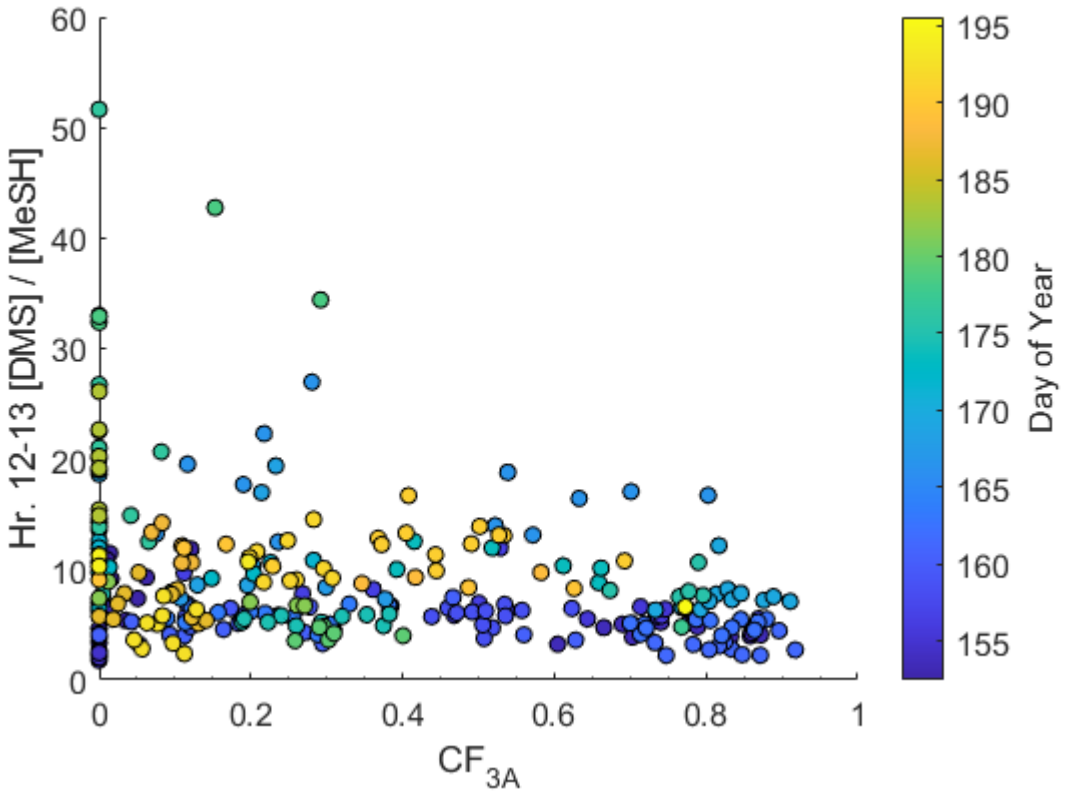

Figure S2: Scatter plot of 5-minute averaged [DMS]/[MeSH] and site-measured 3D cloud fraction during hours 12-13. No dependence in [DMS]/[MeSH] on cloud fraction is observed.

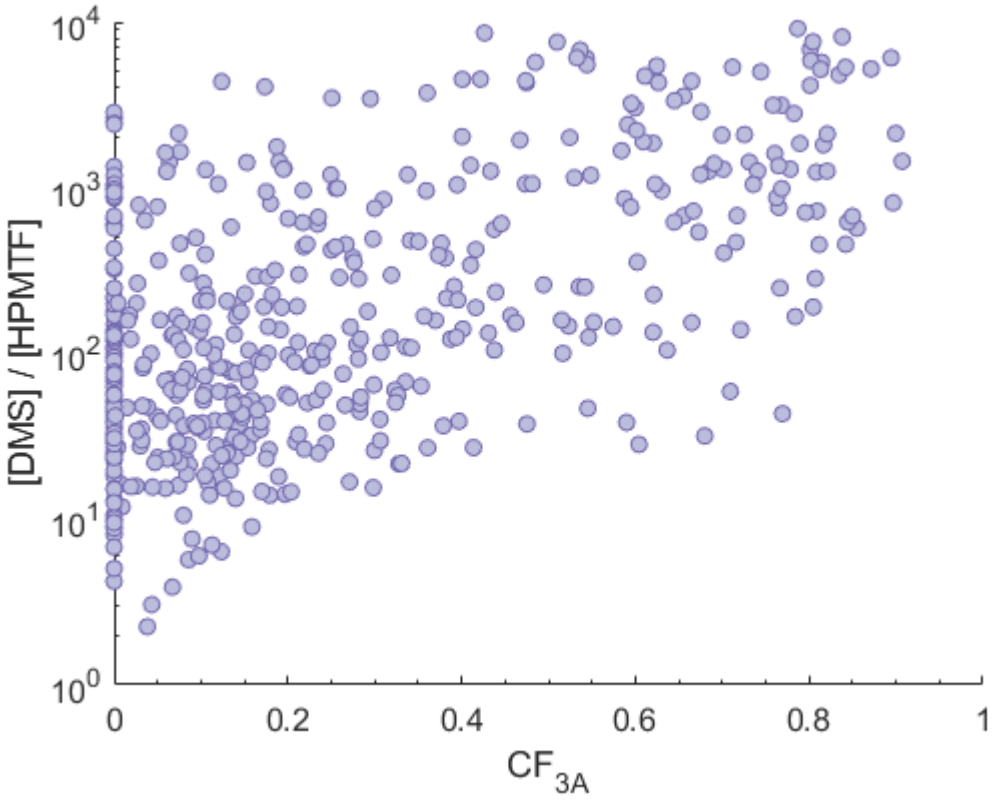

Figure S3: Weak positive relationship between [DMS]/[HPMTF] and CF_{3A} is observed (R^2 = 0.27).

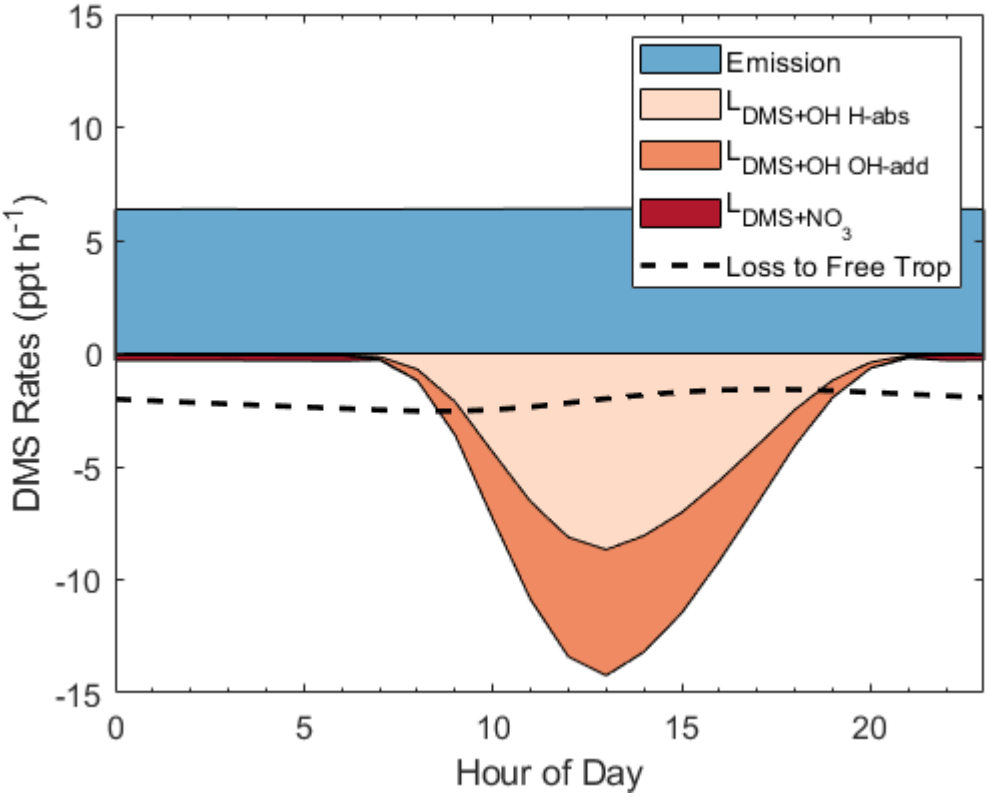

Figure S4: Modelled production and loss rates of DMS in the summertime model with a constant boundary layer height of 1000 m.

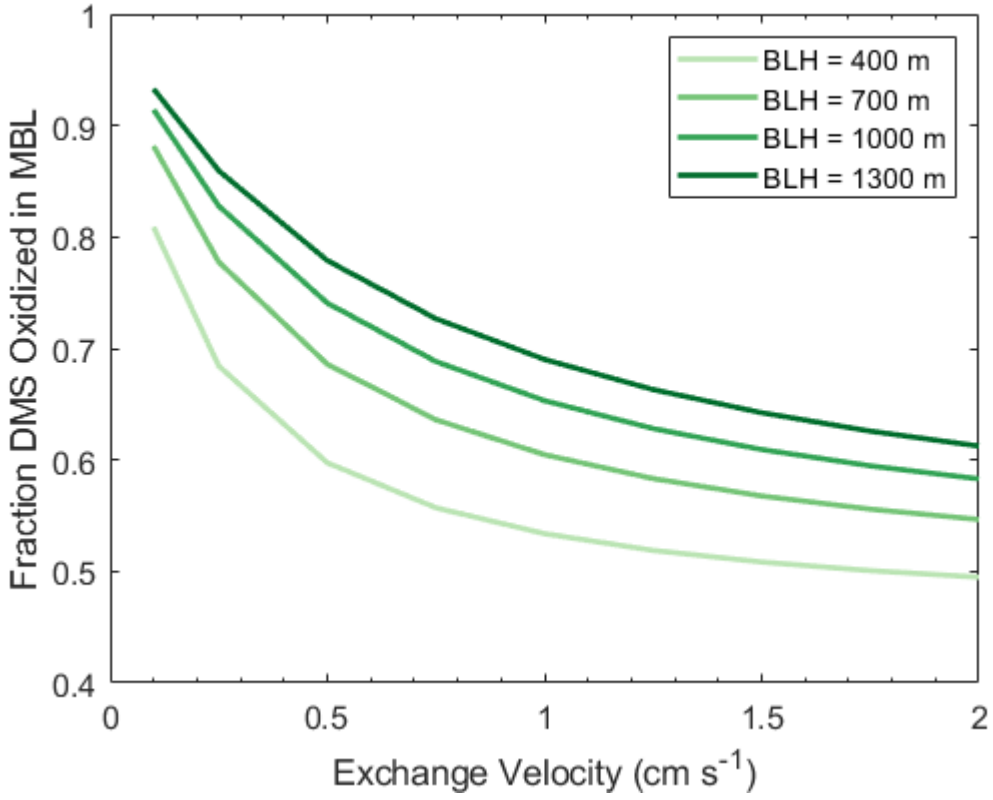

Figure S5: Fraction of DMS oxidized in the boundary layer as a function of exchange velocity at the top of the boundary layer, shown for four different boundary layer heights.

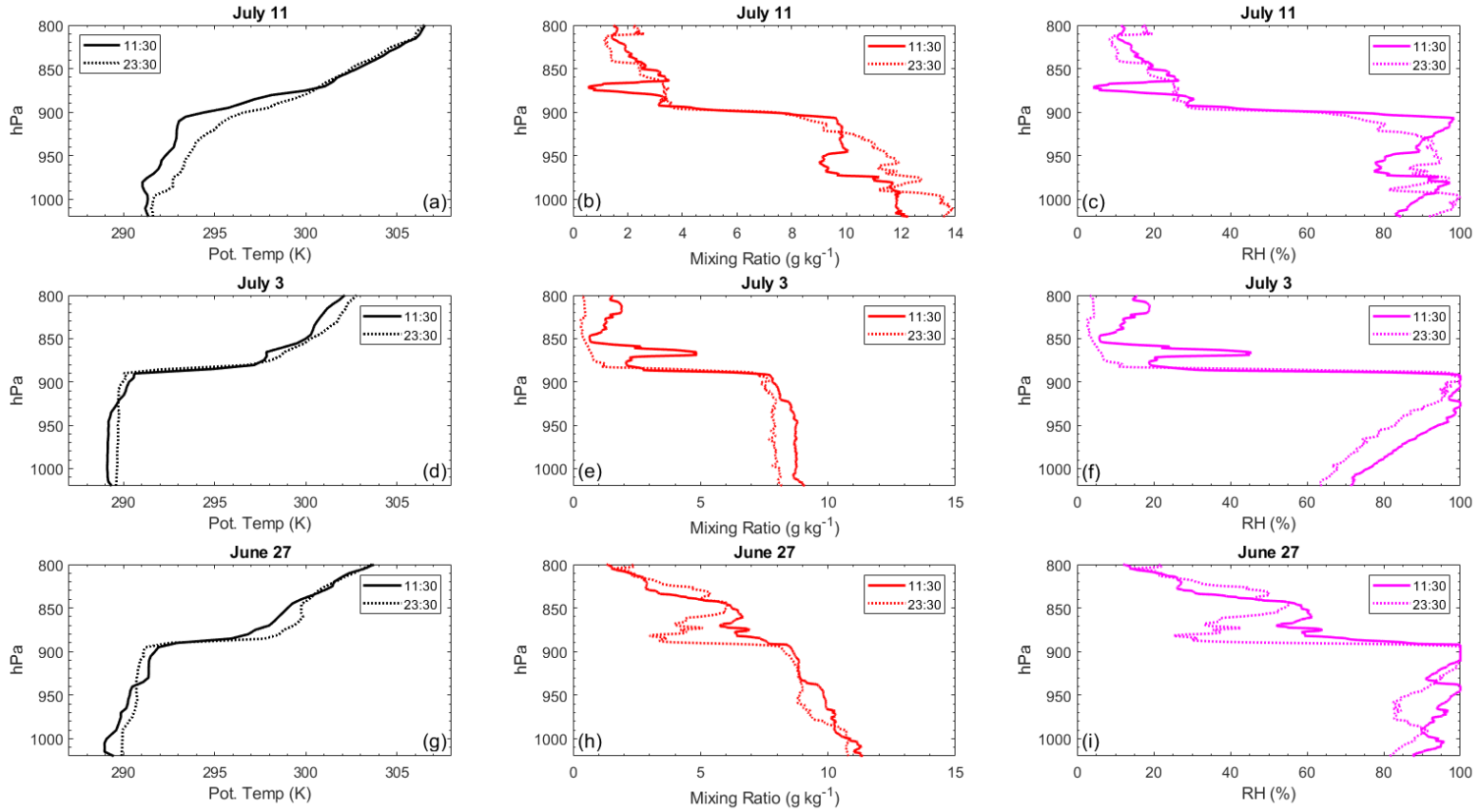

Figure S6: Sonde vertical profiles for days represented in Fig. 3. Potential temperature vertical profile is shown for (a) July 11, (d) July 3, and (g) June 27. Water mixing ratio vertical profile is shown for (b) July 11, (e) July 3, and (h) June 27. Relative humidity vertical profile is shown for (c) July 11, (f) July 3, and (i) June 27.

Table S1: Updated F0AM reactions for DMS and its oxidation products, MeSH, and HPMTF. Only newly added reactions to MCM chemistry are listed here.

MECHANISM	RATE	CITATION
$CH_3SH + OH \rightarrow CH_3S$	k(T) = $(9.9 \times 10^{-12}) \times \exp(360/T)$ cm^3 $molec.^{-1}$ s^{-1}	1
$CH_3SH + NO_3 \rightarrow CH_3S$	k(T) = $(4.4 \times 10^{-13}) \times \exp(210/T)$ cm^3 $molec.^{-1}$ s^{-1}	1
$CH_3SO_2 \rightarrow CH_3 + SO_2$	k(T) = $1.7 \times 10^{15} \times \exp(-8400/T) \times \exp(1800000/T^3)$ cm^3 $molec.^{-1}$ s^{-1}	2
$CH_3SO_2 + O_2 \rightarrow CH_3SO_2O_2$	k(T) = $1.2 \times 10^{-16} \times \exp(1580/T)$ cm^3 $molec.^{-1}$ s^{-1}	2
$CH_3SO_2O_2 \rightarrow CH_3SO_2 + O_2$	k(T) = $1.2 \times 10^{-16} \times \exp(1580/T)/(2.35 \times 10^{-18} \times 5.76 \times 10^{13} \times \exp(-0.0886 \times T))$ cm^3 $molec.^{-1}$ s^{-1}	2
$CH_3SO_3 \rightarrow CH_3 + SO_3$	k(T) = $3 \times 10^{13} \times \exp(-9897/T)$ cm^3 $molec.^{-1}$ s^{-1}	2
$CH_3SCH_2O_2 \rightarrow HPMTF$	k(T) = $2.39 \times 10^9 \times \exp(-7278/T)$ s^{-1}	3
$HPMTF + OH \rightarrow SO_2$	k = $0.87 \times (1.4 \times 10^{-11})$ cm^3 $molec.^{-1}$ s^{-1}	4
$HPMTF + OH \rightarrow OCS$	k = $0.13 \times (1.4 \times 10^{-11})$ cm^3 $molec.^{-1}$ s^{-1}	4
$OCS + OH \rightarrow SO_2$	k(T) = $(7.2 \times 10^{-14}) \times \exp(-1070/T)$ cm^3 $molec.^{-1}$ s^{-1}	1
$HPMTF \rightarrow aerosol$	$\gamma = 0.0016$	5
$HPMTF + deposition$	$v_d = 0.75$ cm s^{-1}	6
$HPMTF + cloud \rightarrow SO_4^{2-}$	Variable rate	This work
$MSIA \rightarrow aerosol$	$\gamma = 0.10$	7
$DMSO \rightarrow aerosol$	$\gamma = 0.10$	8
$MSA \rightarrow aerosol$	$\gamma = 0.13$	8
$DMSO_2 \rightarrow aerosol$	$\gamma = 0.14$	8
$MSIA + deposition$	$v_d = 0.75$ cm s^{-1}	6
$DMSO + deposition$	$v_d = 0.75$ cm s^{-1}	6
$MSA + deposition$	$v_d = 0.75$ cm s^{-1}	6

$DMSO_2$ + deposition	v_d = 0.75 cm s^{-1}	6

1 Burkholder et al., 2019

2 Chen et al., 2023

3 Assaf et al., 2023

4 Jernigan et al., 2022a

5 Jernigan et al., 2022b

6 Vermeuel et al., 2020

7 Hoffmann et al., 2021

8 De Bruyn et al., 1994

References

Assaf, E., Finewax, Z., Marshall, P., Veres, P. R., Neuman, J. A., and Burkholder, J. B.: Measurement of the Intramolecular Hydrogen-Shift Rate Coefficient for the CH3SCH2OO Radical between 314 and 433 K, J. Phys. Chem. A, 127, 2336–2350, https://doi.org/10.1021/acs.jpca.2c09095, 2023.

Burkholder, J. B., Sander, S. P., Abbatt, J., Barker, J. R., Cappa, C., Crounse, J. D., Dibble, T. S., Huie, R. E., Kolb, C. E., Kurylo, M. J., Orkin, V. L., Percival, C. J., Wilmouth, D. M., and Wine, P. H.: Chemical Kinetics and Photochemical Data for Use in Atmospheric Studies, Evaluation No. 19, JPL Publication 19-5, http://jpldataeval.jpl.nasa.gov, 2019.

Chen, J., Lane, J. R., Bates, K. H., and Kjaergaard, H. G.: Atmospheric Gas-Phase Formation of Methanesulfonic Acid, Environ. Sci. Technol., 57, 21168–21177, https://doi.org/10.1021/acs.est.3c07120, 2023.

De Bruyn, W. J., Zahniser, M. S., and Kolb, C. E.: Uptake of gas phase sulfur species methanesulfonic acid, dimethylsulfoxide, and dimethyl sulfone by aqueous surfaces, Journal of Geophysical Research: Atmospheres, 99, 16927–16932, https://doi.org/10.1029/94JD00684, 1994.

Hoffmann, E. H., Heinold, B., Kubin, A., Tegen, I., and Herrmann, H.: The Importance of the Representation of DMS Oxidation in Global Chemistry-Climate Simulations, Geophysical Research Letters, 48, e2021GL094068, https://doi.org/10.1029/2021GL094068, 2021.

Iyer, S., Lopez-Hilfiker, F., Lee, B. H., Thornton, J. A., and Kurtén, T.: Modeling the Detection of Organic and Inorganic Compounds Using Iodide-Based Chemical Ionization, J. Phys. Chem. A, 120, 576–587, https://doi.org/10.1021/acs.jpca.5b09837, 2016.

Jernigan, C. M., Fite, C. H., Vereecken, L., Berkelhammer, M. B., Rollins, A. W., Rickly, P. S., Novelli, A., Taraborrelli, D., Holmes, C. D., and Bertram, T. H.: Efficient Production of Carbonyl Sulfide in the Low-NOx Oxidation of Dimethyl Sulfide, Geophysical Research Letters, 49, e2021GL096838, https://doi.org/10.1029/2021GL096838, 2022a.

Jernigan, C. M., Cappa, C. D., and Bertram, T. H.: Reactive Uptake of Hydroperoxymethyl Thioformate to Sodium Chloride and Sodium Iodide Aerosol Particles, J. Phys. Chem. A, 126, 4476–4481, https://doi.org/10.1021/acs.jpca.2c03222, 2022b.

Vermeuel, M. P., Novak, G. A., Jernigan, C. M., and Bertram, T. H.: Diel Profile of Hydroperoxymethyl Thioformate: Evidence for Surface Deposition and Multiphase Chemistry, Environ. Sci. Technol., 54, 12521–12529, https://doi.org/10.1021/acs.est.0c04323, 2020.